Wind tunnel validation of the CFD OpenFOAM environment of the Formula Student team BCN eMotorsport*

Inca de Ciurana i Montiel
Vehicle Dynamics member and
Brakes and Steering systems responsible

Biel Ruscalleda i Cosculluela
Aerodynamics member and
Computational Fluid Dynamics responsible

Adeline Villardi de Montlaur & José Ignacio Rojas
Professors at the Technical University of Catalonia
(Dated: June 4, 2023)

I. INTRODUCTION

This paper aims to provide valuable insight into the validation by wind tunnel testing of the computational fluid dynamics (hereafter referred to as *CFD*) simulation environment, by the use of OpenFOAM, of BCN eMotorsport, the Formula Student team from Barcelona.

The aerodynamics department performs simulations via OpenFOAM to test and refine designs, as well as perform thermal simulations, at a very low expense, and within a very short time span. OpenFOAM is a free, open-source CFD software based on Linux and C++. Once a final design is manufactured, however, one must ensure its simulations and thus performance predictions meet reality. In aerodynamics this is most commonly done by wind tunnel testing. That is concretely what has been done in this study.

II. THE WIND TUNNEL

The measurements have been done using the wind tunnel at EETAC, Castelldefels, Barcelona. It is a semi-open wind tunnel, with a closed chamber and an open return circuit (See Fig. 1). Its anatomy is as follows:

1. Firstly, the air enters through a contraction and flow conditioning chamber. Here, the air from the room is accelerated, in a controlled manner, up to the desired speed, thus gaining kinetic energy.

2. Then, it passes through the test chamber. The chamber of the tunnel is 40 cm wide, 40 cm tall and 60 cm long. Here, the tested geometry must meet certain requirements for good flow behaviour and analysis. Firstly, the frontal area of the model must be less than 10 % of the chamber's frontal area. And secondly, the wingspan of the model must be less than 80 % of the width of the chamber.

3. The disturbed air then passes through the diffuser, which slows down the air regaining potential energy in a controlled way.

4. Lastly, the air is able to recirculate in a closed loop by virtue of the drive system, which consists of a fan of adaptable angular velocity. For the experiment, the air has been set to 13.67 m/s, as that is the average velocity that the car runs through the very tight and twisty Formula Student circuits.

To measure the data, a three-component scale has been used, measuring lift (or for race cars, *downforce*), drag and pitch moment. The data has been obtained by means of a data acquisition program and then post-processed in Excel and Matlab.

As, in this case, the model is a real flap and obviously up to scale, there is no need to consider the principle of dynamic similarity of wind tunnel testing.

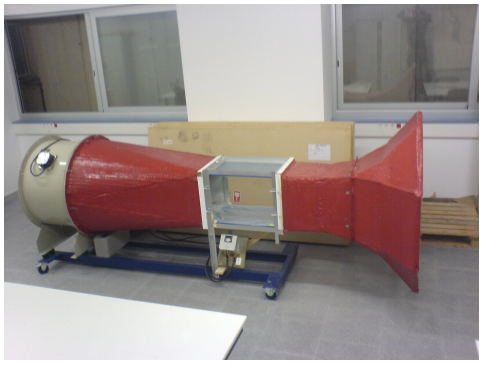

FIG. 1: Wind tunnel at EETAC

* https://bcnemotorsport.upc.edu/home/

III. GEOMETRIES STUDIED

Two different geometries have been issued. The first is an extrusion of an airfoil profile, thus becoming a flap, which belongs to the side wing assembly of this year's vehicle. The second consists of the same flap together with an endplate. These have been designed in SolidWorks and exported to STL (Standard Triangle Language) files for the simulations. In order to hold in place the assembly to the vehicle, 3D printed PAHT CF15 inserts are incorporated. Inside the tunnel, the bunch is bolted to a cylindric bar, which is then pinched by the three-component balance of the wind tunnel. These are the main specifications:

- Chord of 15 cm and wingspan of 22.5 cm
- Projected frontal area of 124.19 cm^2
- Planform area of 318.37 cm^2
- There is no fixed angle of attack.

The requirements for good wind tunnel behaviour and simulation convergence can be easily checked to be met.

FIG. 2: CAD render of both geometries. Without endplate (left), with endplate (right)

In the case of the flap, the assembly consists of two carbon fiber skins, a Rohacell core and two PAHT CF15 3D printed inserts. The manufacturing procedure started with the lamination of pre-preg twill carbon fiber to a negative, upper skin mold and its lower skin counterpart. Once the skin cured in the autoclave, two 10 mm thick Rohacell rib-like cores were machined to the correct geometry, and the inserts were printed. In order to stick together these parts, epoxy resin together with fiberglass microspheres served as the gluing medium, ensuring good geometry with press molding.

The endplate was fabricated with TeXtreme spread tow carbon fiber, which together with a machined, 5 mm thick Rohacell core, two PAHT CF15 3D printed inserts and epoxy resin mixed with fiberglass microspheres, was press molded and thus cured. The endplate was finally drilled at the according hole positions for bolts to tighten the flap-endplate complex.

The objective of placing an endplate to the flap is to study how it affects the pressure distribution, vorticity and thus downforce and drag of the bunch. An increase in downforce is to be expected, as high and low pressures have a physical barrier that prevents them from merging and forming an energetic vortex. A vortex at the other end of the assembly is expected, as no endplate is placed. The expected critical angle of attack is of 17.2º. As a reminder, lift (or *downforce*) and drag forces are computed as:

$$F_L = \frac{1}{2}\rho S C_L v^2 \quad F_D = \frac{1}{2}\rho S C_D v^2$$

where ρ is the density of air, which is selected to be 1.225 kg/m^3 as the tunnel is situed at sea level, v^2 is the squared relative velocity between air and geometry, and SC_L and SC_D are the surface times coefficient of lift and coefficient of drag, respectively. These depend on the shape of the body, and are the main unknowns in this study.

IV. SIMULATION ENVIRONMENT

There have been two phases of simulation for the development of this study. The first was the correct geometry acquisition, with proper design procedures and thus the final geometry was chosen. However, attention will be directed towards the second phase, where the aim is to computationally recreate the real wind tunnel environment, and thus predict what is measured in reality.

The simulations have been run at CSUC, a supercomputing company which sponsors the team providing capable hardware to withstand the high computational demand of fluid simulations. The pipeline of the simulation environment of the team is as follows:

1. blockMeshDict: here one defines the domain of the wind tunnel, as well as general cell sizes and shapes, and as such an initial mesh is built. The solver will run through each and every cell, in many iterations, and apply the different equations that describe the air's behaviour.
2. decomposePar: the different iterations can be processed and stored in parallel, being this study one of these cases.
3. snappyHexMeshDict: next up, one tailors the initial mesh to the imported geometry, by the use of castellatedMesh, snap and addLayers. These three steps, in order, first approximate the shape of the surface to the mesh, then cut any cells inside the surface, and lastly add the prism layers (those cells closest to the surface).
4. simpleFoam: once the mesh is fully defined, the solver kicks in. simpleFoam is one of them, which is used for steady-state, incompressible, turbulent flow problems, just like at the issued wind tunnel. It uses the Reynolds-averaged Navier-Stokes (RANS) equations and the finite volume method.

5. reconstructPar: it gathers and merges the field data from the different individual processor files into a single file, reconstructing the original field as if it were computed on a single processor.

6. postProcessing: lastly, postProcessing scripts facilitate the user's analysis of the results, either by providing .txt, .vtk, .png, *et cetera* files, containing all sorts of useful data. This is entirely done by the team, mostly in Python.

Herein lie the most relevant parameters employed for this simulation:

- Iterations: 1500 on 16 cores in parallel
- Velocity: 13.67 m/s
- Air density: 1.225 kg/m^3
- Model: k-ω Shear Stress Transport (SST), with turbulence consideration
- blockMesh type: hexahedral
- blockMesh domain: $(x, y, z) = (1.64, 0.4, 0.4)$ m (three chords in front, seven behind)
- Inlet patch and conditions: frontal face. uniform (0 0 0) U, zeroGradient p
- Outlet patch and conditions: back face. $internalField U, $internalField p
- Wall patch and conditions: side, top and bottom faces. slip U, zeroGradient p
- Geometry patch conditions: noSlip U, zeroGradient p
- Prism or surface layers: 5
- Expansion ratio: 1.2
- First layer thickness: 0.0001 m (0.1 m)
- y^+ [min, max, avg]: $2.3 \cdot 10^{-8}$, 282, 2.21

These items, and mainly those related to the mesh, have been carefully tailored by means of a mesh refinement and convergence study. Regarding the latter, the simulation is set to finish after 1500 iterations. It has been found that, at a bit less than that, the slope of the regression of values is low enough for it to be considered stable.

V. RESULTS

A. Simulation results

Simulations were run on both geometries, with varying angles of attack. The analysis has been done using postProcessing tools in Paraview, and *readme* text files which portray the necessary information in an automatic manner. The numerical results are portrayed in Fig. 6, at the following subsection.

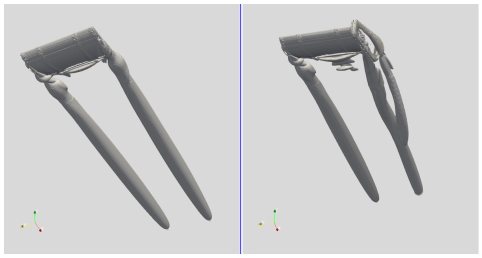

FIG. 3: Vorticities of the two geometries

As seen above, the vorticity from the outer edge of the flap is severely reduced, but two new vortices (one from the bottom of the endplate, and another from the top) are generated, although provoked by non-downforce generating regions. This is yet again seen in the mean velocity field cross-section view of Fig. 4 up next. The top case shows the vortex mean velocity field, and the bottom case shows how the vortex is severely reduced. The cross-section views are as close to the endplate (or the edge) as it gets. The endplate silhouette can just be distinguished in the bottom case.

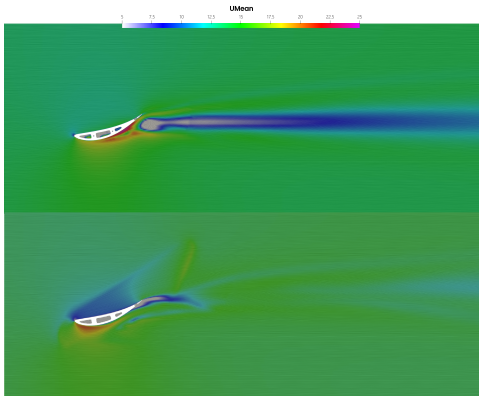

FIG. 4: Mean velocity fields for the two geometries. No endplate (top), with endplate (bottom)

The last qualitative analysis is regarding the critical angle of attack. As can be seen in Fig. 5, flow separation at 17.2 degrees is starting to occur near the trailing edge, and the addition of an endplate has little to no effect.

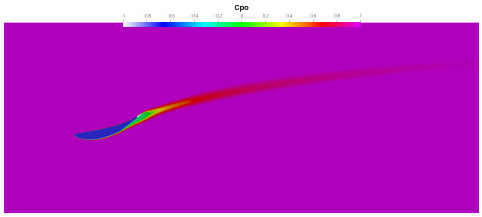

FIG. 5: Pressure coefficient distribution across Y

As an observation, note that there is air inside the flap. That is because the core isn't spread throghout the

entire flap, but consists of two different ribs with nothing in between. Also note that Fig. 5 portrays C_p. In the team, C_p is used as a way to visualize downforce:

$$p_L = \frac{F_L}{S} = \frac{\frac{1}{2}\rho S C_L v^2}{S} = \frac{1}{2}\rho C_L v^2 = \rho C_L C_p$$

Up next lie useful truncated data from the simulation without endplate, at an angle of 17.2 degrees:

- Total execution time: 15 hours and 40 minutes
- Total real simulation time: 58 minutes and 42 seconds
- Number of cells: 4 200 000
- Fifth refinement level cells: 834 000
- Fourth refinement level cells: 1 460 000
- Third refinement level cells: 1 900 000
- Max aspect ratio: 20.38
- Max face skewness: 8.43
- Mesh non-orthogonality [max, avg]: 65.7, 4.08

What is most relevant about these results is the maximum face skewness, which has a relatively high value. A total of 10 highly skew faces were detected, which could impair the quality of the results, but considering that there were a total of 12.9 million faces, the results are satisfying. Moreover, log.checkMesh portrayed checks to every relevant mesh parameter. Lastly, all mesh parameters were the same for the eight simulations. As such, only one case has been analysed to this level as the other seven contain equal characteristics.

B. Wind tunnel results and validation

The wind tunnel measurements are plotted as continuous lines in Fig. 6 and Fig. 7.

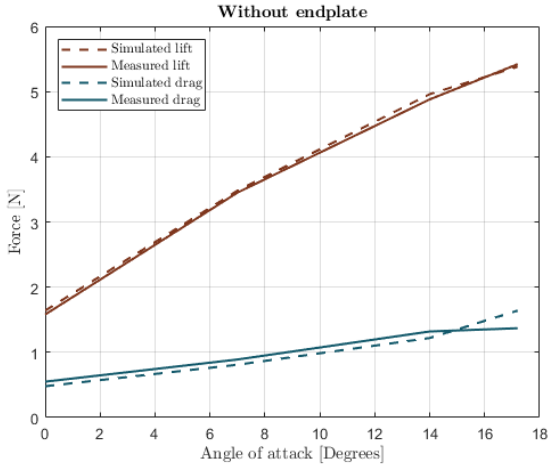

FIG. 6: Simulated and measured lift and drag forces, without endplate

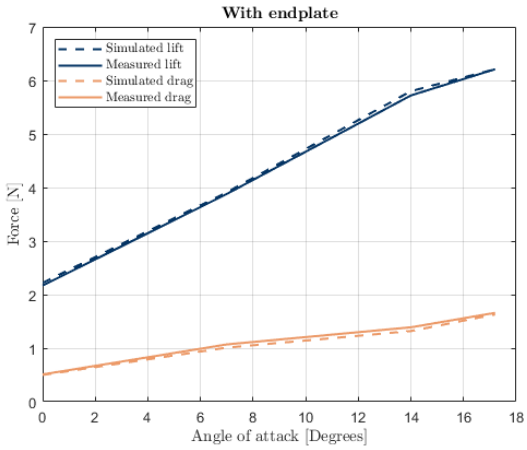

FIG. 7: Simulated and measured lift and drag forces, with endplate

Angle calibration has been done in order to properly adjust the values. As seen, downforce is increased when an endplate is present, and drag is a bit higher than that which is simulated. This is due to manufacturing inaccuracies, as molds have tolerances, different thermal expansions and press molding disadjustments. Other sources can be mesh and solver imprecision, and balance errors.

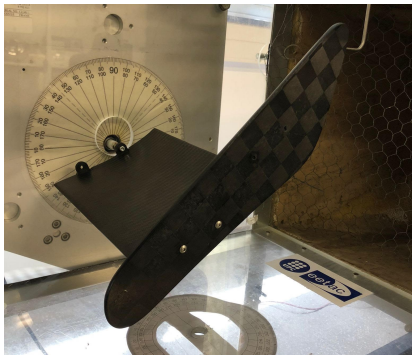

FIG. 8: Testing chamber with the flap and endplate

VI. CONCLUSIONS

This paper evaluates the behaviour of an aerodynamic component with CFD and includes a validation of the model with the use of a wind tunnel. Two different configurations have been tested and all the predictions have been concluded valid, according to the data obtained in the measurements and simulations, with little discrepancies mostly due to human error. However, the results are satisfying as the data fits the theory that lays behind it.

VII. REFERENCES

Katz, J. (1995). Race Car Aerodynamics: Designing For Speed. Bentley Publishers.